Journal of Sound and Vibration 329 (2010) 5058–5069

Contents lists available at ScienceDirect

Journal of Sound and Vibration

journal homepage: www.elsevier.com/locate/jsvi

# On the dynamics of a novel ocean wave energy converter

B. Orazov, O.M. O'Reilly *, Ö. Savaş

*Department of Mechanical Engineering, University of California at Berkeley, Berkeley, CA 94720, USA*

ARTICLE INFO

*Article history:*
Received 20 May 2009
Received in revised form
5 May 2010
Accepted 6 July 2010
Handling Editor: M.P. Cartmell

ABSTRACT

Buoy-type ocean wave energy converters are designed to exhibit resonant responses when subject to excitation by ocean waves. A novel excitation scheme is proposed which has the potential to improve the energy harvesting capabilities of these converters. The scheme uses the incident waves to modulate the mass of the device in a manner which amplifies its resonant response. To illustrate the novel excitation scheme, a simple one-degree of freedom model is developed for the wave energy converter. This model has the form of a switched linear system. After the stability regime of this system has been established, the model is then used to show that the excitation scheme improves the power harvesting capabilities by 25–65 percent even when amplitude restrictions are present. It is also demonstrated that the sensitivity of the device's power harvesting capabilities to changes in damping becomes much smaller when the novel excitation scheme is used.

© 2010 Elsevier Ltd. All rights reserved.

## 1. Introduction

Ocean waves are a source of renewable energy with energy densities far exceeding those of any other renewable source, such as solar or wind power [1]. Wave energy converters (WEC) belong to a class of mechanical devices that harvest the energy stored in the ocean waves and transform it into a more useful form, typically electrical. Seminal works in this area include Salter's paper [2] which appeared during the oil crisis in 1974, and the subsequent papers by Evans [3,4] and Mei [5] showing how WECs of the type discussed by Salter could extract 100 percent of the incident wave energy. Since Salter's work, many categories of WECs have appeared [6]. The primary type of WEC of interest here are known as wave activated bodies (WAB). In these devices, waves force the device into oscillatory motions (mainly heave, pitch, and roll), and a power takeoff system (PTO) uses these motions to drive a generator. These devices are usually implemented off-shore in deep water, where the waves are stronger and a greater motion range is possible.

The Wavebob,[1] a floating buoy (cf. Fig. 1), and Pelamis,[2] a floating snake, are two of the most well-known examples of such wave energy converters. As illustrated in the patent [7], Wavebob uses two floats, which are connected to each other by a hydraulic PTO and move relative to each other due to a phase offset in the waves' forcing. The device also allows active changes to the mass (and thus the natural frequency) of both floats by filling underwater reservoirs with water in order to match the dominant exciting frequency of the waves, thus ensuring that the system is at or near resonance as often as possible. Resonance is desirable because the power harnessed through a hydraulic PTO depends on (in this case) the vertical velocity of the floats relative to each other. Since the wave climate in deep sea can stay relatively constant for

* Corresponding author. Tel.: +1 510 642 0877; fax: +1 510 643 5599.
*E-mail address:* oreilly@me.berkeley.edu (O.M. O'Reilly).
[1] http://www.wavebob.com
[2] http://www.pelamiswave.com

0022-460X/$ - see front matter © 2010 Elsevier Ltd. All rights reserved.
doi:10.1016/j.jsv.2010.07.007

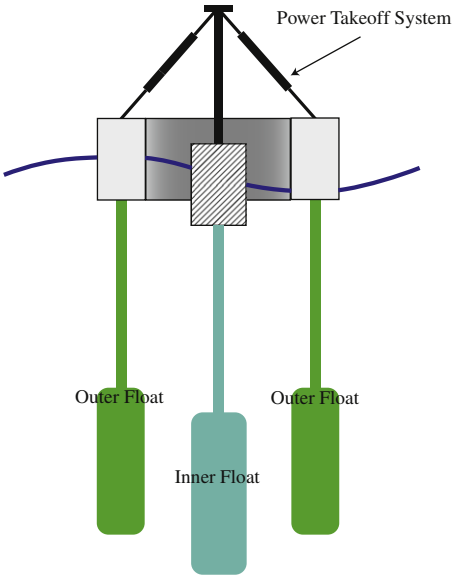


**Fig. 1.** Schematic of a wave energy converter. The relative motion of the inner and outer floats is used to generate electricity.

hours, the mass adjustments are made infrequently. Further, the resonant frequencies are usually of the order of 0.5 Hz and lower.

To further improve on the aforementioned resonant excitation and the energy harvesting capabilities of WAB-type WECs, we propose a novel excitation scheme in this paper. The scheme has similarities to, but is distinct from, the familiar parametric excitation of an oscillator: a scheme that has a long and celebrated history (see [8–11] and references therein). Dating to the seminal paper by Rugar and Grütter [12] it has been known that parametric excitation can produce mechanical amplification in the response of a resonator. This amplification has been used in a variety of MEMS oscillators (see [13] and references therein), and has also been discussed for use in a type of WEC featuring oscillating water columns [14]. Here, we propose a novel excitation method for WECs which extends the idea of using the mass of added water as ballast and also produces a mechanical amplification. However, instead of long-term mass adjustments, water intake and disposal happens as rapidly as two times per motion cycle. Further, the distinction between the resulting excitation and a parametric excitation lies in the fact that the variation in the mass for the novel excitation scheme is state-dependent.[3] The excitation scheme is realizable and we have designed a mechanical system that results in an nearly square wave modulation of the mass parameter. Using a simple one-degree of freedom model, we will show that the amplification of the resonant response can be used to significantly increase the power harvesting capabilities of a WEC.

In the next section of this paper, the novel excitation scheme is presented. We then introduce a simple dynamics model for our system, formulate the equations of motion and discuss a solution procedure for them. Although the resulting model is linear, it is also a switched system, and we need to examine the boundedness of its output to bounded inputs. That is, we need to examine its bounded-input–bounded-output (BIBO) stability. In Section 4, our stability analysis, which is based on a one-dimensional Poincaré map, is presented. We show that the BIBO stability of the system features a balance between mass modulation and damping. Following the stability analysis, we look at the average harnessed power per cycle and examine the efficacy of our excitation scheme in Section 5. Finally, we subject the system to an amplitude constraint and find the damping values which enable a maximization of harnessed power. Even in the presence of amplitude limitations, we find that an increase in energy harvesting of up to 65 percent is possible. The paper closes with a discussion of unresolved issues and future proposed work on the excitation scheme.

## 2. A novel excitation scheme for wave energy converters

The excitation system we propose here mimics a square wave modulation of the mass of the WEC. This modulation occurs at twice the temporal frequency of the incident waves and results in a state-dependent excitation. The excitation system depends crucially on a water intake system which traps water for the first quarter of the incident wave's periodic motion, releases it for the second quarter of the wave's motion, traps it for the third quarter of the wave's motion, and releases it once more for the final quarter of the wave's motion.

[3] By way of contrast, the dynamics of a parametrically excited oscillator whose inertia is varied as a prescribed function of time is considered in [9,10].

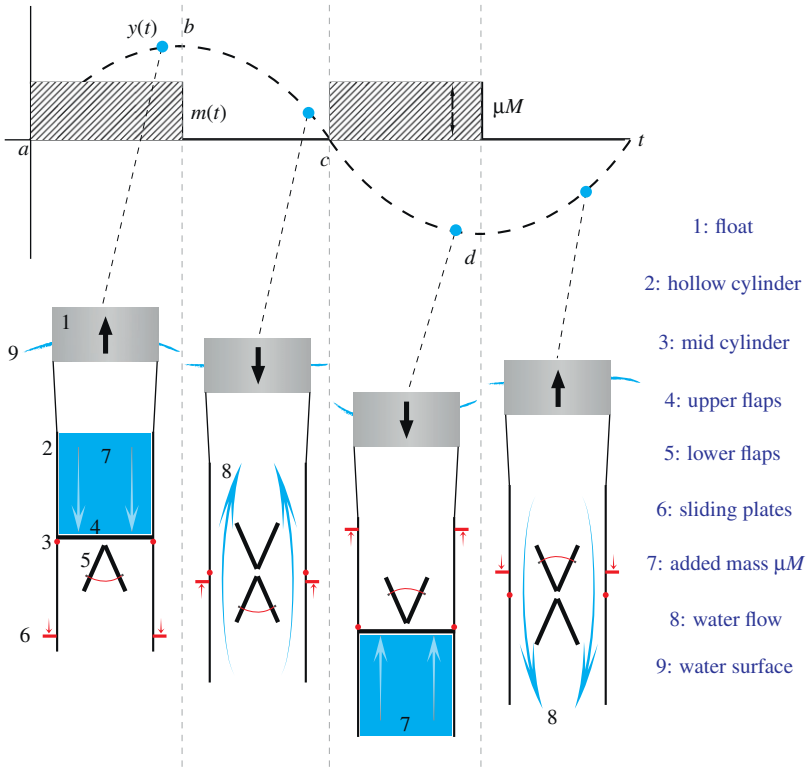


**Fig. 2.** Illustration of the operation of the water intake mechanism. An animation of the mechanism can be found at [http://me.berkeley.edu/~bayram/wec/water_intake_animation.html].

Referring to Fig. 2, the water intake system is composed of a submerged (at all times) hollow cylinder labeled (2) in Fig. 2, open at both ends and rigidly attached to the surface float (1) that is excited by the waves. Inside the cylinder, located near its vertical midpoint (3), are two pairs of centrally hinged butterfly flaps. The upper flaps (4) are able to swing between horizontal and nearly vertical up positions, while the lower flaps (5) can only swing between horizontal and nearly vertical down positions. The exact vertical orientations would depend on system design considerations, such as geometry, drag vs. sensitivity tradeoff, etc.

When in the horizontal 'closed' position, each pair of flaps covers the entire cross section of the cylinder, thereby blocking off water flow through the inside of the cylinder. As water cannot flow through the cylinder, it gets trapped in one of its halves (in the upper half when the float/cylinder system is moving up, and in the lower half during downward motion of the system), thereby creating the desired added mass effect. It should be noted that the mechanism is arranged in such a way as to allow at most one set of flaps to be closed at any given time. The remaining parts of the water intake system, as labeled in Fig. 2, are the horizontal plates (6), sliding on the outside of the cylinder due to water pressure from the top or bottom, depending on the direction of motion. When passing through the midpoint (3) of the cylinder, the sliding plates can lock or unlock the flaps (4) or (5) in their 'open' configurations. In Fig. 2 the locked state is indicated by an arc between the flaps. The locking mechanism can range from a simple mechanical device to an electronically controlled brake.

During a typical period of the system's motion (shown as a dashed sine wave), the water intake operates as follows. At point labeled *a* in Fig. 2 the sliding plates (6) pass through the midpoint (3) of the cylinder, locking lower flaps (5) in the open configuration and unlocking upper flaps (4) from their previously open configuration. Because the cylinder is moving up, the water pressure above the upper flaps is greater than below them. This forces the upper flaps to swing downward into the horizontal configuration and block off the cylinder's cross section. In turn, this leads to the added mass effect, due to the water (7) trapped in the upper half of the cylinder. The device remains in this state until it reaches point *b*, the topmost position in the cycle. Note that by the time *b* is reached, the horizontal plates (6) are near the bottom of the cylinder.

At *b*, the direction of motion is reversed, with the entire system accelerating down. Now the water pressure below the upper flaps is greater than above them, which forces the flaps to swing up and allows water to flow through the cylinder. The lower flaps (5) are still locked in the open state, so they cannot close, despite the increased water pressure from below. Therefore, no mass is added during the quarter cycle between *b* and *c*. Meanwhile, the sliding plates (6) are moving up relative to the cylinder.

At point *c* the downward motion continues, reaching the maximum vertical speed. As the plates (6) again pass through the midpoint (3) of the cylinder, they lock the upper flaps (4) in the open state and unlock the lower flaps (5), allowing

them to close under increased water pressure from below. This now traps the volume of water in the lower half of the cylinder, again leading to the added mass effect. The system continues to move in this state until point $d$, by which time the sliding plates (6) have moved to the top of the cylinder.

At $d$ the direction of motion is again reversed and the system starts to accelerate up. This forces the lower flaps (5) to open, and water flow through the cylinder is again established, resulting in no added mass. The horizontal plates (6) are now moving down relative to the cylinder, and when point $a$ is reached in the next cycle, they pass through the midpoint (3), locking the lower flaps (5) open and unlocking the upper flaps (4) to close. The cycle then repeats. It should be noted that although the sliding horizontal plates (6) move up and down relative to the cylinder (2), their absolute position in the water remains approximately constant. Effectively, they act as inertial plates and remain stationary in the water.

## 3. A simple model for the WEC

To show the efficacy of the novel excitation scheme, we first develop and analyze the simplest possible model of a heaving buoy WEC. The model is a single degree-of-freedom damped, harmonically excited linear oscillator, whose mass $m$ is modulated in time (cf. Fig. 3). The system features a square wave modulation in the mass parameter. An amount of water mass is added to the system for two of the quarter cycles, and no water mass is added during the other two quarter cycles. Referring to Fig. 2, the precise instants where water is added or released is governed by the instants when either the displacement $y$ or velocity $\mathrm{d}y/\mathrm{d}t$ of the oscillator are zero. The effects of the ocean waves are modeled by an external harmonic excitation. Following the work of Salter et al. [2,3,5], we model the power takeoff as a damping element and this element is incorporated into the damping term in the model. The goal of the model is to examine how the power absorbed by the oscillator's PTO can be optimized using the state-dependent modulation of the mass. Due to the mass intake and release, we find that the model may also be conveniently described as a hybrid or switched linear system.

It is straightforward to show that the governing equations for the simple model are the following system:

$$M(1+\mu)\frac{\mathrm{d}^2y}{\mathrm{d}t^2}+C\frac{\mathrm{d}y}{\mathrm{d}t}+Ky=F\sin(\omega_f t),\quad y\frac{\mathrm{d}y}{\mathrm{d}t}>0,$$

$$M\frac{\mathrm{d}^2y}{\mathrm{d}t^2}+C\frac{\mathrm{d}y}{\mathrm{d}t}+Ky=F\sin(\omega_f t),\quad y\frac{\mathrm{d}y}{\mathrm{d}t}<0. \tag{1}$$

Here, $y$ is the displacement of the mass, $M$ is the default system mass, $\mu M$ is the added mass, $C$ is the damping coefficient (a sum of viscous damping from the water and external damping from the PTO), $K$ is a spring constant of hydrodynamic origin, and $F$ is the magnitude of the external excitation force (attributed to water waves) which is varying sinusoidally at a frequency $\omega_f$. We refer to $\mu$ as the mass modulation parameter.

The system (1) is an example of a switched system where the switching conditions are state-dependent. The set of differential equations (1) needs to be supplemented by jump conditions at the locations where $y\,\mathrm{d}y/\mathrm{d}t=0$. These locations, which are referred to as the switching set, are along the $y=0$ and $\mathrm{d}y/\mathrm{d}t=0$ axes in the $y$–$\mathrm{d}y/\mathrm{d}t$ plane. For the simple model, we shall assume that $y(t)$ and $\mathrm{d}y/\mathrm{d}t$ are both continuous functions of time at the switching set. Continuity of $y(t)$ is easy to justify on the grounds that the motion of the oscillator is physically realistic. On the other hand, the continuity of $\mathrm{d}y/\mathrm{d}t$ assumes that the intake and release of the added mass $\mu M$ does not result in impulsive loading.

We non-dimensionalize (1) by defining a time $\tau=t\sqrt{K/M}$ which is used to help transform (1) into

$$\ddot{x}+2\delta_1\dot{x}+\omega_{n_1}^2x=f_1\sin(\omega\tau),\quad \dot{x}x>0,$$

$$\ddot{x}+2\delta_2\dot{x}+x=f_2\sin(\omega\tau),\quad \dot{x}x<0. \tag{2}$$

The $(\dot{})$ indicates a differentiation with respect to $\tau$ and the new parameters and fields are given by

$$x=\frac{y}{L},\quad f_1=\omega_{n_1}^2f_2,\quad \delta_1=\frac{\delta_2}{(1+\mu)},\quad \omega_{n_1}=\sqrt{\frac{1}{1+\mu}},$$

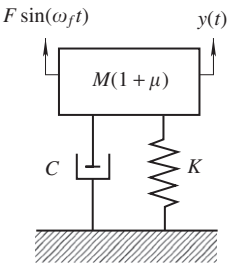


**Fig. 3.** Schematic for the single degree-of-freedom linear oscillator.

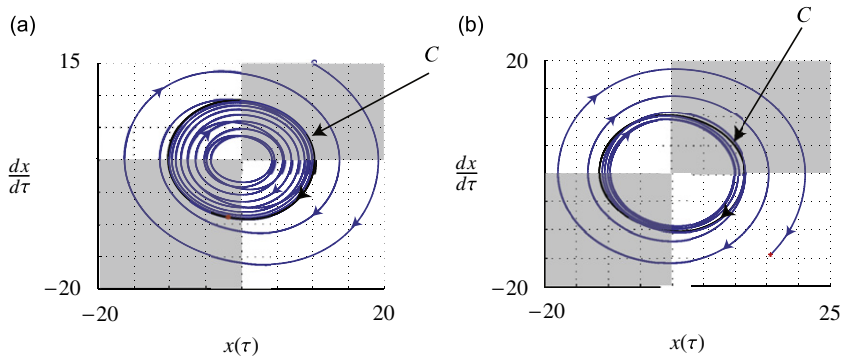


**Fig. 4.** Examples of limit cycles $\mathcal{C}$ and transient responses in their neighborhoods for the forced system (2) with $f$=1, $\mu=0.3$ and $\omega=0.9$: (a) stable limit cycle ($\delta=0.08$), and (b) unstable limit cycle ($\delta=0.01$).

$$f_2=f=\frac{F}{KL},\quad \delta_2=\delta=\frac{C}{2\sqrt{KM}},\quad \omega=\omega_f\sqrt{\frac{M}{K}}, \tag{3}$$

where $L$ is a suitable length scale.[4] The solutions to (2) are classical:

$$x=\begin{cases} x_1(\tau) & \text{when } \dot{x}x>0,\\ x_2(\tau) & \text{when } \dot{x}x<0. \end{cases} \tag{4}$$

Here,

$$x_1(\tau)=e^{-\delta_1\tau}(A_1\cos(\omega_{d_1}\tau)+B_1\sin(\omega_{d_1}\tau))+X_1\sin(\omega\tau-\phi_1),$$

$$x_2(\tau)=e^{-\delta_2\tau}(A_2\cos(\omega_{d_2}\tau)+B_2\sin(\omega_{d_2}\tau))+X_2\sin(\omega\tau-\phi_2), \tag{5}$$

with

$$X_1=\frac{f_1}{\sqrt{(\omega_{n_1}^2-\omega^2)^2+(2\delta_1\omega)^2}},$$

$$X_2=\frac{f_2}{\sqrt{(1-\omega^2)^2+(2\delta_2\omega)^2}}, \tag{6}$$

and

$$\omega_{d_1}=\omega_{n_1}\omega_{d_2},\quad \omega_{d_2}=\sqrt{1-\delta_2^2},$$

$$\phi_1=\tan^{-1}\left(\frac{2\delta_1\omega}{\omega_{n_1}^2-\omega^2}\right),\quad \phi_2=\tan^{-1}\left(\frac{2\delta_2\omega}{1-\omega^2}\right). \tag{7}$$

For a given motion of the system, the constants $A_i$ and $B_i$ are prescribed by matching the solutions $x_1(\tau)$ and $x_2(\tau)$ at the switching boundaries.

It is tempting to assume that the solution to (2) will always be bounded if the input is bounded (i.e., BIBO stable). However, because we are dealing with a switched system, it is well-known that this is not necessarily the case (see [15–17]). Two representative examples of stable and unstable responses of the system are shown in Fig. 4. The limit cycles shown in these figures are the steady-state response of the system. From numerical integrations of (2) we observe that for a fixed value of damping $\delta_2$ if the mass modulation parameter $\mu$ is sufficiently small, then the response of the system will be BIBO stable. However, if $\mu$ is sufficiently large then the response will no longer have this property. Clearly, it is of interest to determine the regime where the system is BIBO stable. We now turn to this issue.

## 4. Bounded-input–bounded-output stability of the system

Of primary interest is to determine the parameters for BIBO stability of the switched system (2). For a given excitation $f_2\sin(\omega\tau)$, we observe that the system has a steady-state response which is a limit cycle (cf. Fig. 4). We wish to determine the conditions for the stability of this limit cycle or equivalently the BIBO stability of the system.

[4] For example, $L$ could be chosen to be the maximum allowable displacement of the mass–spring–damper system.

Developing analytical criteria for the BIBO stability of the system is challenging. Several results are available and feature the construction of a Lyapunov function for a discrete-time equivalent system (see [18,19]). In this paper, we follow an alternative approach. First, we restrict attention to the unforced system and establish the stability criterion for its trivial equilibrium. To do this, we construct a one-dimensional Poincaré map. The resulting stability criteria are presented as a curve in the $\mu-\delta$ plane. We then examine the stability of the limit cycles observed in the forced system using an extensive series of numerical integrations. After these results are compiled, it becomes evident that the stability results for the unforced system provide a useful coarse estimate on the parameter regime for the BIBO of the forced system.

### 4.1. Stability of the trivial equilibrium

The unforced system is governed by the equations (from (2)):

$$\ddot{x}+2\delta_1\dot{x}+\omega_{n_1}^2 x=0, \quad \dot{x}x>0,$$

$$\ddot{x}+2\delta_2\dot{x}+x=0, \quad \dot{x}x<0, \tag{8}$$

respectively. Clearly this system has a single trivial equilibrium. To examine the stability of the trivial equilibrium, we solve (8) over a time interval $T$. Referring to Fig. 5, it is easy to see that this allows us to define a Poincaré map $\Phi$:

$$z_{n+1}=\Phi(z_n), \tag{9}$$

where

$$z_n=(0,\dot{x}(nT))\in\mathcal{B}, \quad n\in\mathbb{Z}^+. \tag{10}$$

The switching boundary $\mathcal{B}$ is

$$\mathcal{B}=\{(x,\dot{x})|x=0 \text{ and } \dot{x}>0\}. \tag{11}$$

The time $T$ is the time it takes for a solution of the differential equation to return to $\mathcal{B}$. For linear stability of the trivial equilibrium, we require the one-dimensional map $\Phi$ to be contractive.

After some work with the solutions of (8), we find that $\Phi$ is a simple linear mapping:

$$z_{n+1}=p^2 z_n. \tag{12}$$

The function $p$ is defined by

$$p=\frac{1}{\omega_{n_1}}e^{-\delta_2 T_2}e^{-\delta_1 T_1}=e^{-\delta_2 T_2}e^{-\delta_1 T_1}\sqrt{1+\mu}, \tag{13}$$

where the times $T_1$ and $T_2$ are found by solving the transcendental equations

$$\frac{\delta_1}{\omega_{n_1}\omega_{d_1}}\tan(\omega_{d_1}T_1)=1,$$

$$\frac{\delta_2}{\omega_{d_2}}\tan(\omega_{d_2}T_2)=-1. \tag{14}$$

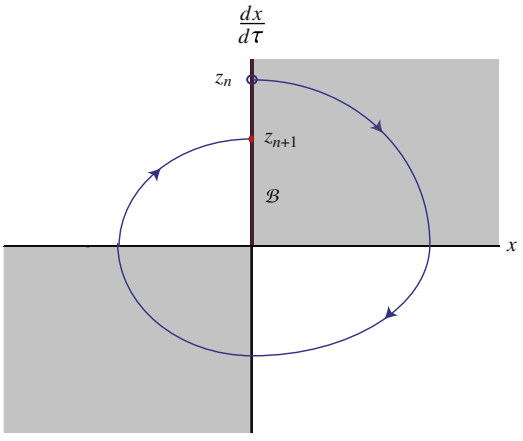


**Fig. 5.** Schematic of the phase flow of (8) and how it is used to construct the Poincaré map $\Phi:\mathcal{B}\to\mathcal{B}$.

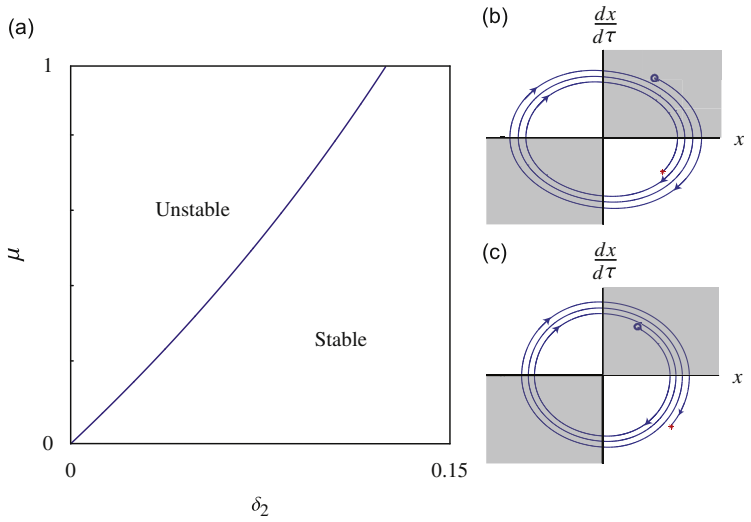


**Fig. 6.** Stability region for the trivial equilibrium of (8) is shown in (a). Representative phase portraits for stable and unstable cases of (8) are shown in (b) and (c), respectively.

That is,

$$T_1 = \frac{1}{\omega_{d_1}}\left(\arcsin\left(\sqrt{1-\frac{\delta_1^2}{\omega_{n_1}^2}}\right)\right),$$

$$T_2 = \frac{1}{\omega_{d_2}}\left(\pi-\arcsin\left(\sqrt{1-\delta_2^2}\right)\right),$$

$$T = 2T_1 + 2T_2. \tag{15}$$

For stability, we require $|p| < 1$.

To determine the stability of the trivial equilibrium, we seek points where $|p| < 1$. This calculation leads to the stability region shown in Fig. 6. Clearly, there is a delicate balance here between mass modulation $\mu$ and damping $\delta_2$. If the latter is sufficiently large, then stability will always be guaranteed. Otherwise, under perturbation, the trivial equilibrium will become unstable. In physical terms, if one adds and extracts too much mass then it can become unstable if insufficient damping is present.

### 4.2. Numerical investigation for BIBO stability

When the system is harmonically excited (i.e., $f_{1,2}\sin(\omega\tau)\neq 0$), a limit cycle is observed. An explicit expression for $x(t)=x_L(t)$ corresponding to the limit cycle can be determined by piecewise matching of the solutions (5) to (2), and computing the time periods when the solution transits between elements of the switching set (which is defined by $x\dot{x}=0$). The equations needed to determine $x_L(t)$ are nonlinear and must be solved numerically. An alternative method of finding the limit cycle is to numerically integrate (2) forwards (backwards) in time to find the stable (unstable) limit cycle. This is the approach we followed. One result that is evident from these simulations is that the $x_L(t)$ will contain contributions from the terms with frequencies $\omega_{d_{1,2}}$ in (5).

To examine the stability of the limit cycle, we numerically integrate (2) for various values of the excitation frequency $\omega$. Of particular interest is the case $\omega=\omega_{\text{peak}}$, which corresponds to the excitation frequency which results in the largest displacement of the system. The value of $\omega_{\text{peak}}$ depends on $\mu$ and $\delta_2$ and must be determined numerically. As can be seen from Fig. 7, the response of the system to this excitation frequency determines the BIBO stability regime. The stability criterion for the unforced case from Fig. 6 is also shown in Fig. 7. The proximity of the criteria for $f_2=0$ and $\omega=\omega_{\text{peak}}$ is remarkable.

## 5. The efficacy of mass modulation for energy harvesting

Of crucial interest is the amount of energy harvested by the oscillator compared to the energy which is incident on the oscillator due to the forcing $f\sin(\omega_f t)$. To compute the harvested energy it suffices to calculate the average power per cycle of the external forcing that the system can harness. Here, the harnessed power [2,3,5,20,21] is taken to be proportional to

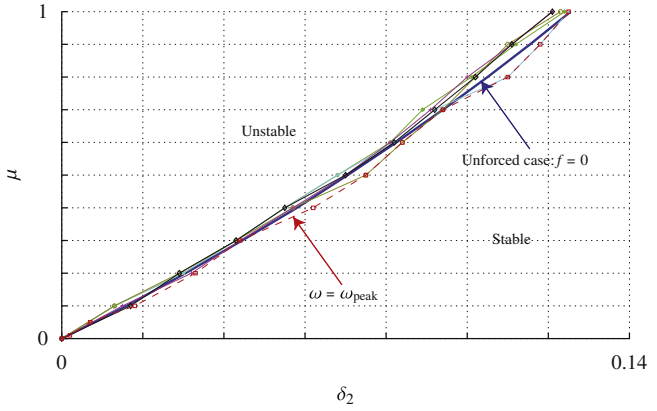


**Fig. 7.** BIBO stability regions for the forced system (2) for various excitation frequencies $\omega$. The solid line is the stability criterion for the trivial equilibrium of the unforced system (cf. Fig. 6(a)). In this figure, $\square : \omega = \omega_{peak}$ $* : \omega = 0.8$, $\star : \omega = 0.85$, $\circ : \omega = 0.9$, $| : \omega = 0.95$, and $\diamond : \omega = 1.0$.

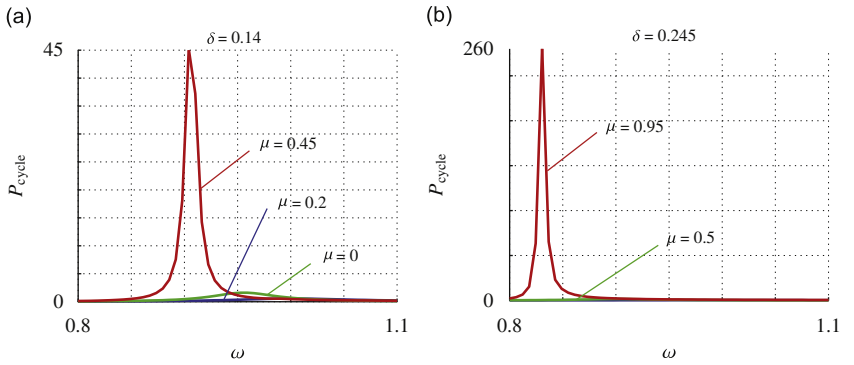


**Fig. 8.** Average power per cycle $P_{cycle}$ as a function of driving frequency $\omega$ for selected values of damping factor $\delta = C/2\sqrt{KM}$ as indicated on the figure. Maximum power per cycle for each case is shown in Table 1.

the damping coefficient $\delta = \delta_2 = C/2\sqrt{KM}$ and the velocity squared.[5] That is, the average power harvested is

$$P_{avg} = \frac{\delta}{T}\int_0^T \dot{x}^2 \, d\tau. \tag{16}$$

The average power per cycle is then given by dividing $P_{avg}$ by the number of cycles during this time interval. First, we note that

$$T_{cycle} = \frac{2\pi}{\omega}, \quad \omega = \omega_f\sqrt{\frac{M}{K}}. \tag{17}$$

Then, the average power per cycle $P_{cycle}$ is

$$P_{cycle} = \frac{P_{avg}}{T_{cycle}} = \frac{\delta}{T \cdot T_{cycle}}\int_0^T \dot{x}^2 \, d\tau. \tag{18}$$

Simulating the system for a range of frequencies and computing $P_{cycle}$, gives the results shown in Fig. 8. When computing these results, values of $\mu$ and $\delta$ corresponding to BIBO stability of the system were selected.

The results shown in Fig. 8 were obtained using $\mu$ values corresponding to 0, 20, 45, 50 and 95 percent of the total mass $M$, respectively. For higher values of the mass modulation parameter $\mu$ the plots show a marked increase in power produced by the excited system, compared to the regular case (i.e., the case $\mu = 0$ shown in Fig. 8(a)). The maximum power per cycle $P_{cycle_{max}}$ values for each of the cases presented in Fig. 8 are given in Table 1. These results demonstrate that the mass modulation can significantly improve the energy harvesting capabilities of the oscillator. It should also be noted that in contrast to a regular system where $\mu = 0$, the power peak for the mass modulated system lies to the left of the $\omega = 1$ line.

[5] This damping coefficient $\delta$ is the sum of the damping provided by the PTO and the hydrodynamic damping. We tacitly assume that the latter is constant in our analyses, and assume that the variation of $\delta$ can be achieved by altering the parameters of the PTO.

**Table 1**
Maximum power per cycle $P_{\text{cycle}_{\max}}$ for various values of damping factor $\delta = C/2\sqrt{KM}$ and mass modulation parameter $\mu$.

| $P_{\text{cycle}_{\max}}$ | $\delta = 0.14$ | $\delta = 0.245$ |
|---|---|---|
| $\mu = 0$ | 0.56 | 0.32 |
| $\mu = 0.2$ | 1.6 | – |
| $\mu = 0.45$ | 45 | – |
| $\mu = 0.50$ | – | 1.55 |
| $\mu = 0.95$ | – | 260 |

All presented combinations of $\delta$ and $\mu$ result in a stable system.

Since $\omega = \omega_f/\sqrt{K/M}$ does not take into account the mass modulation $\mu$ term (which would lower the value of the resonant frequency), effectively $\omega = 1$ lies above the resonant frequency for the system with the novel excitation scheme.

## 6. The maximum power that can be harvested when the amplitude of motion is limited

The dramatic increase in absorbed power happens primarily at low values of damping, and correspondingly high amplitudes of oscillation. In practice, this would not be achievable, as there would inevitably exist a number of restrictions (such as stroking, slamming and force restrictions) on the maximum allowable response amplitude. To explore this issue further, we now examine the power which can be harvested if the response amplitude of the system is restricted.

In this section, we discuss an analytical expression for the optimum damping coefficient $\delta$ as a function of driving frequency $\omega$ which maximizes $P_{\text{cycle}}$ at every $\omega$. We start our analysis with the case where there is no mass modulation (i.e., $\mu = 0$), and then supplement these results with numerically obtained values of the damping coefficients that maximize the harvested power for the cases where the mass is modulated using the novel excitation scheme.

For practical reasons, the system's response amplitude often needs to be limited to some maximum value $X_{\max}$. Using this value in $(6)_2$ and solving for $\delta$ yields

$$\delta_{\min} = \frac{1}{2\omega}\sqrt{f^2 - X_{\max}^2(1-\omega^2)^2}. \tag{19}$$

This expression gives the lower bound on the value of $\delta$ necessary to keep the response amplitude at or below $X_{\max}$. Yet, for $\omega \le \sqrt{1-f/X_{\max}}$ or $\omega \ge \sqrt{1+f/X_{\max}}$, it is evident that $\delta_{\min}$ given by (19) has no real component, meaning that the harnessed power in (18) is zero. This also means that for these frequency ranges, the system would not be able to oscillate at an amplitude of $X_{\max}$ while absorbing power from the damper. Thus, we need to find a value of $\delta$ that will produce the maximum power at each driving frequency $\omega$, regardless of amplitude constraints. To do this, we use $(6)_2$ to establish an expression for $\dot{x}^2$ in (18) and then differentiate the resulting integral with respect to $\delta$. This is equivalent to maximizing the function $S$ as a function of $\delta$ where

$$S(\delta) = \frac{f^2\omega^2\delta}{(1-\omega^2)^2 + 4\delta^2\omega^2}. \tag{20}$$

Solving for the values of $\delta$ where $\partial S/\partial\delta = 0$, we find two values depending on the value of $\omega$:

$$\delta_A^* = \frac{1-\omega^2}{2\omega}, \quad \delta_B^* = \frac{\omega^2-1}{2\omega}. \tag{21}$$

Examining $\partial^2 S/\partial\delta^2(\delta = \delta_{A,B}^*)$ and evaluating it at $\delta_{A,B}^*$ we find that it is negative. Thus $\delta_{A,B}^*$ yield maximum values of harvested power. Clearly, $\delta_{A,B}^* \to 0$ as $\omega \to 1$, so in the vicinity of the resonant frequency these values are not feasible. Therefore, instead of looking at a single expression for optimal damping, we need to simultaneously take into account (19) and (21). Fig. 9 shows a plot of $\delta_{A,B}^*$ and $\delta_{\min}$ as functions of $\omega$.

We note that for $\omega < \omega_A^*$, $\delta_A^* > \delta_{\min}$. Since $\delta_A^*$ is set to maximize harnessed power without regard to amplitude limits, and it exceeds the minimum value of damping needed to keep the response amplitude bounded, this is the value of the damping coefficient that should be used in this frequency range. Likewise, for $\omega > \omega_B^*$, $\delta_B^* > \delta_{\min}$, so $\delta_B^*$ should be set as the damping coefficient. But in the range $\omega_A^* \le \omega \le \omega_B^*$, $\delta_{\min}$ is the lowest damping value at which $X_{\max}$ is not exceeded. Hence $\delta_{\min}$ is the damping setting of choice in this intermediate frequency range. Equating (19) and $(21)_1$, we can solve for the values of $\omega_A^*$ and $\omega_B^*$:

$$\omega_A^* = \sqrt{1 - \frac{f}{\sqrt{2}X_{\max}}}, \quad \omega_B^* = \sqrt{1 + \frac{f}{\sqrt{2}X_{\max}}}. \tag{22}$$

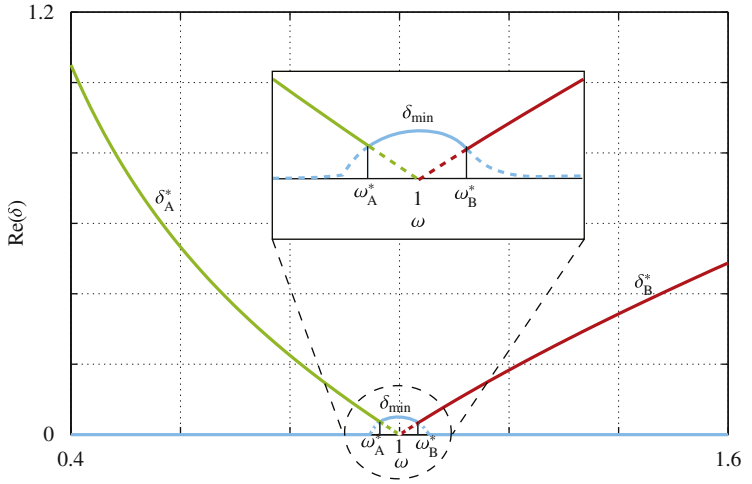


**Fig. 9.** Real positive parts of damping factors given by (19) and (21) as functions of driving frequency $\omega$. The plot for optimal $\delta$ is shown as a solid line. $\delta_{\min}$ was computed using $X_{\max}=1$ and $f=0.1$. Note that the peak for $\delta_{\min}$ occurs slightly below $\omega=1$. This is because the peak response amplitude (but not power, as per [21]) for a damped system occurs at $\omega_p=\omega_n\sqrt{1-2\delta^2}$, where $\omega_n$ is the undamped natural frequency (which is equivalent to $\omega=1$ in our model).

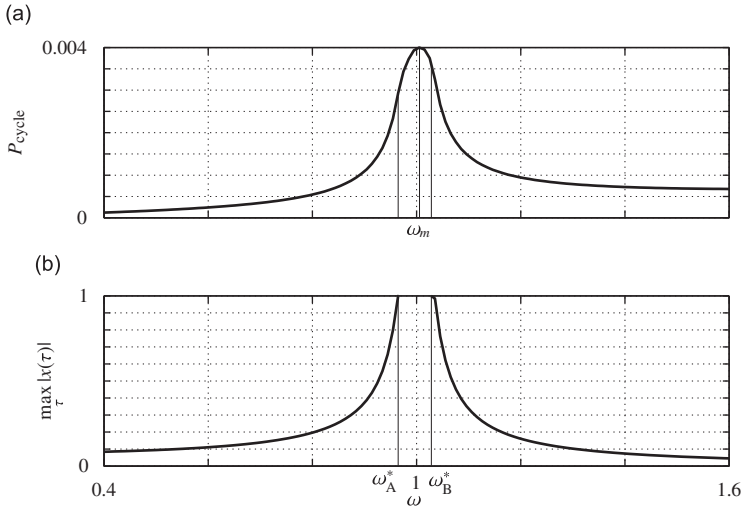


**Fig. 10.** (a) Average power harvested per cycle and (b) response amplitude as functions of driving frequency $\omega$ using the damping values given by (23). Simulations were performed using $f=0.1$ and $X_{\max}=1$.

Hence, the optimal damping coefficient is given by

$$\delta_{\text{opt}}=\begin{cases}\dfrac{1-\omega^2}{2\omega}, & 0\le\omega<\omega_A^*,\\ \dfrac{1}{2\omega X_{\max}}\sqrt{f^2-X_{\max}^2(1-\omega^2)^2}, & \omega_A^*\le\omega<\omega_B^*,\\ \dfrac{\omega^2-1}{2\omega}, & \omega_B^*\le\omega.\end{cases}\tag{23}$$

As an illustration, Fig. 10 shows the power harvested per cycle and maximum response amplitude as functions of frequency $\omega$ when $\delta_{\text{opt}}$ is used. Note that the peak in power occurs at a frequency $\omega_m$ to the right of $\omega=1$. This is due to the fact that while response amplitude is capped at $X_{\max}$ for both frequencies, the value of the velocity $\dot{x}$ is higher at $\omega_m$. Indeed, the ratio of peak power to that at $\omega=1$ is proportional to the ratio of these two frequencies.

Next, we perform a set of simulations to determine optimal damping values at each excitation frequency $\omega$ that maximize harnessed power per cycle. Unlike the cases presented in Fig. 8, we impose an amplitude constraint of $X_{\max}=1$ at all frequencies. The simulation program then sweeps through a range of damping values $\delta$ at each frequency, computes the power and maximum amplitude, and selects the damping value at which $P_{\text{cycle}}$ is the largest while $\max_\tau|x(\tau)|\le 1$.

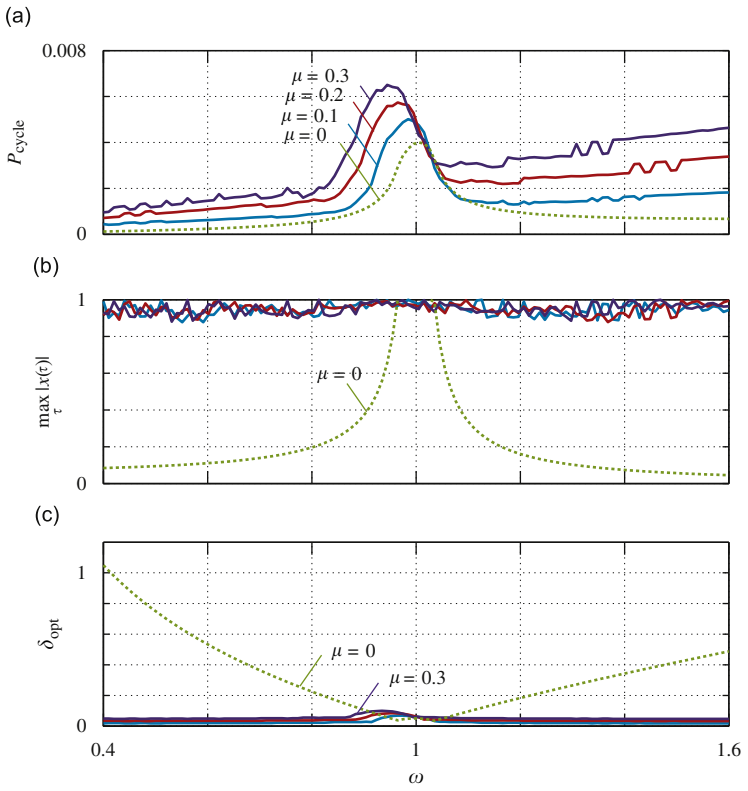


**Fig. 11.** (a) Average power per cycle, (b) maximum response amplitude, and (c) optimal damping coefficients $\delta_{\text{opt}}$ as functions of driving frequency $\omega$ for $\mu$ values of 0, 0.1, 0.2 and 0.3 as indicated on the figure. The case where mass is not modulated is shown with a dashed line. Simulations were performed using $f$=0.1 and $X_{\text{max}}$=1.

**Table 2**
Maximum power per cycle $P_{\text{cycle}_{\text{max}}}$ and the associated optimal values of damping $\delta_{\text{opt}}$ for plots shown in Fig. 11.

| | $\mu = 0$ | $\mu = 0.1$ | $\mu = 0.2$ | $\mu = 0.3$ |
|---|---|---|---|---|
| $P_{\text{cycle}_{\text{max}}}$ | 0.004 | 0.005 | 0.0057 | 0.0065 |
| $\omega$ at $P_{\text{cycle}_{\text{max}}}$ | 1.005 | 0.9849 | 0.9647 | 0.9445 |
| $\delta_{\text{opt}}$ at $P_{\text{cycle}_{\text{max}}}$ | 0.0495 | 0.0659 | 0.0828 | 0.0975 |

The results are presented in Fig. 11 for $\mu$ values of 0, 0.1, 0.2 and 0.3, while maximum power and optimal damping values are shown in Table 2. An inspection of Fig. 11(a) reveals that when the amplitude is restricted, mass modulation no longer provides the large improvements in harvested power that Fig. 8 showed. The improvements in maximum harnessed power at $\mu$ values of 0.1, 0.2 and 0.3 are 25, 42.5 and 62.5 percent, respectively. The gains would be larger if $X_{\text{max}}$ were larger.

Looking at Fig. 11(b), we observe that for all cases where mass modulation is present, the maximum response amplitude hovers around the $X_{\text{max}}$=1 mark. This means that amplitude constraints take precedence over power maximization. It is of interest to compare this to the case of the constant mass system which is shown in Fig. 11(a)–(c) and labeled $\mu = 0$. For this case, the maximum amplitude drops off on both sides of $\omega = 1$ to maximize power, as given by (21). Finally, Fig. 11(c) shows that there is little variation in the optimal damping coefficients for the cases where $\mu \neq 0$. Again, this is due to the need to keep the peak amplitude below $X_{\text{max}}$ for all frequencies. It also implies that a WEC featuring the novel excitation system has the advantage for the designer in having a small variation in the optimal damping parameter when compared to the traditional system.

## 7. Conclusions and future work

The intent of this paper is to demonstrate the manner in which the novel excitation scheme can expand the potential and efficiency of ocean wave energy converters. We have chosen to model the system as simply as possible and neglected several effects: most notably a detailed modeling of the hydrodynamic effects. It has been known since the work of Cummins [22] that these effects will introduce memory-type terms into the governing equations of motion. The precise

values of these terms depends on the geometry of the WEC [23]. The resulting delay-differential equations of motion are notoriously difficult to analyze (see [24–26] and references therein), but this task will be the subject of our future work.

The second main object of our future work will be the development and wave tank testing of a scaled model for a WEC featuring the novel excitation scheme presented in this paper. Such a model is also needed in order to characterize the dissipation resulting from the excitation scheme and to quantify the significance of higher-order terms in our model. Eventually, before a full implementation of the method, a full hydrodynamic simulation of the WEC, including all of its components must be carried out. Such a simulation will be a major undertaking.

## Acknowledgments

The authors would like to take this opportunity to thank Professor Steven Shaw for his helpful discussions on parametric excitation, Professor N. Sri Namachchivaya for his helpful suggestions about switched systems, Professor Ron Yeung for his help with wave energy converters, and the reviewers for their constructive criticisms. This research was supported by a grant from the University of California at Berkeley-King Abdullah University of Science and Technology (UCB-KAUST) Academic Excellence Alliance.

## References

[1] 2007 Survey of Energy Resources, World Energy Council. URL ⟨http://www.worldenergy.org⟩.
[2] S.H. Salter, Wave power, *Nature* 249 (1974) 720–724 URL ⟨http://dx.doi.org/10.1038/249720a0⟩.
[3] D.V. Evans, A theory for wave-power absorption by oscillating bodies, *Journal of Fluid Mechanics* 77 (1) (1976) 1–25 URL ⟨http://dx.doi.org/10.1017/S0022112076001109⟩.
[4] D.V. Evans, Wave-power absorption by systems of oscillating surface pressure distributions, *Journal of Fluid Mechanics* 114 (1982) 481–499 URL ⟨http://dx.doi.org/10.1017/S0022112082000263⟩.
[5] C.C. Mei, Power extraction from water waves, *Journal of Ship Research* 20 (2) (1976) 63–66.
[6] J. Brooke, *Wave Energy Conversion*, Elsevier, Oxford, UK, 2003.
[7] W. Dick, Wave energy converter, U.S. Patent number 6857266, issued in February 2005.
[8] K. Billah, On the definition of parametric excitation for vibration problems, *Journal of Sound and Vibration* 270 (1–2) (2004) 450–454 URL ⟨http://dx.doi.org/10.1016/S0022-460X(03)00408-5⟩.
[9] E.I. Butikov, Parametric excitation of a linear oscillator, *European Journal of Physics* 25 (4) (2004) 535–554 URL ⟨http://dx.doi.org/10.1088/0143-0807/25/4/009⟩.
[10] E.I. Butikov, Parametric resonance in a linear oscillator at square-wave modulation, *European Journal of Physics* 26 (1) (2005) 157–174 URL ⟨http://dx.doi.org/10.1088/0143-0807/26/1/016⟩.
[11] D. Watt, M.P. Cartmell, Externally loaded parametric oscillator, *Journal of Sound and Vibration* 170 (3) (1994) 339–364 URL ⟨http://dx.doi.org/1006/jsvi.1994.1067⟩.
[12] D. Rugar, P. Grütter, Mechanical parametric amplification and thermomechanical noise squeezing, *Physical Review Letters* 67 (6) (1991) 699–702 URL ⟨http://dx.doi.org/10.1103/PhysRevLett.67.699⟩.
[13] J.F. Rhoads, J.N. Miller, S.W. Shaw, B.F. Feeny, Mechanical domain parametric amplification, *Journal of Vibration and Acoustics* 130 (6) (2008) 061006-1–061006-7 URL ⟨http://dx.doi.org/10.1115/1.2980382⟩.
[14] A. Olvera, E. Prado, S. Czitrom, Parametric resonance in an oscillating water column, *Journal of Engineering Mathematics* 57 (1) (2007) 1–21 URL ⟨http://dx.doi.org/10.1007/s10665-006-9048-z⟩.
[15] M. Johansson, Piecewise Linear Control Systems, Ph.D. Thesis, Lund Institute of Technology, 1999.
[16] D. Liberzon, S.A. Morse, Basic problems in stability and design of switched systems, *IEEE Control Systems Magazine* 19 (1999) 59–70.
[17] D. Liberzon, *Switching in Systems and Control, Systems & Control: Foundations & Applications*, Birkhäuser, Boston, MA, 2003.
[18] J.M. Gonçalves, Regions of stability for limit cycle oscillations in piecewise linear systems, *IEEE Transactions on Automatic Control* 50 (11) (2005) 1877–1882 URL ⟨http://dx.doi.org/10.1109/TAC.2005.858674⟩.
[19] M. Rubensson, B. Lennartson, Global convergence analysis for piecewise linear systems applied to limit cycles in a DC/AC converter, *Proceedings of the American Control Conference*, vol. 2, Anchorage, Alaska, May 8–10, 2002, pp. 1272–1277. URL ⟨http://dx.doi.org/10.1109/ACC.2002.1023195⟩.
[20] G. De Backer, M. Vantorre, R. Banasiak, J. De Rouck, C. Beels, H. Verhaeghe, Performance of a point absorber heaving with respect to a floating platform, *7th European Wave and Tidal Energy Conference*, Porto, 2007.
[21] N.G. Stephen, On energy harvesting from ambient vibration, *Journal of Sound and Vibration* 293 (1–2) (2006) 409–425 URL ⟨http://dx.doi.org/10.1016/j.jsv.2005.10.003⟩.
[22] W.E. Cummins, The impulse response function and ship motions, *Schiffstechnik* 9 (17–18) (1962) 101–109.
[23] J.V. Wehausen, The motion of floating bodies, *Annual Review of Fluid Mechanics* 3 (1971) 237–268 URL ⟨http://dx.doi.org/10.1146/annurev.fl.03.010171.001321⟩.
[24] E. Kristiansen, A. Hjulstad, O. Egeland, State-space representation of radiation forces in time-domain vessel models, *Ocean Engineering* 32 (17–18) (2005) 2195–2216 URL ⟨http://dx.doi.org/10.1016/j.oceaneng.2005.02.009⟩.
[25] M. Ó'Cathán, B.J. Leira, J.V. Ringwood, J.-C. Gilloteaux, A modelling methodology for multi-body systems with application to wave-energy devices, *Ocean Engineering* 35 (13) (2008) 1381–1387 URL ⟨http://dx.doi.org/10.1016/j.oceaneng.2008.05.005⟩.
[26] R. Taghipour, T. Perez, T. Moan, Hybrid frequency–time domain models for dynamic response analysis of marine structures, *Ocean Engineering* 35 (7) (2008) 685–705 URL ⟨http://dx.doi.org/10.1016/j.oceaneng.2007.11.002⟩.